AMERICAN SCIENTIFIC PUBLISHERS

Science of Advanced Materials
Vol. 6, pp. 1814–1819, 2014
(www.aspbs.com/sam)

ARTICLE

$Y_2O_3:Eu^{3+}/C_3N_4$ Composite Nanotubes: Synthesis, Characterization, and Novel Luminescence Properties

Ying Li[1], Xi Cao[1], Guofeng Wang[1,*], Bingyu Xu[1], and Jisen Zhang[2,*]

[1]*Key Laboratory of Functional Inorganic Material Chemistry, Ministry of Education, School of Chemistry and Materials Science, Heilongjiang University, Harbin, 150080, China*
[2]*Changchun Institute of Optics, Fine Mechanics and Physics, Chinese Academy of Sciences, Changchun 130033, China*

ABSTRACT

We successfully prepared $Y_2O_3:Eu^{3+}/C_3N_4$ composite nanotubes by combining the hydrothermal with chemisorption method for the first time. The infrared spectra indicated that the C–N (1238 cm^{-1}) stretching vibration peak moved to a higher wavenumber with increasing the amount of $Y_2O_3:Eu^{3+}$, suggesting the formation of $Y_2O_3:Eu^{3+}/C_3N_4$ composite nanotubes. The charge transfer bands showed a little blue-shift after compositing with C_3N_4 in the excitation spectra of $Y_2O_3:Eu^{3+}/C_3N_4$ composite nanotubes monitored at 615 nm. More importantly, the sharp lines originate from Eu^{3+} f–f electron transitions almost vanished in the excitation spectra of $Y_2O_3:Eu^{3+}/C_3N_4$ composite nanotubes, which was attributed to the interaction between C_3N_4 and $Y_2O_3:Eu^{3+}$. The decay curve of $Y_2O_3:Eu^{3+}$ and $Y_2O_3:Eu^{3+}/C_3N_4$ composite nanotubes can be fitted with the biexponential function well. The luminescence lifetimes of $Y_2O_3:Eu^{3+}$ increased by combining C_3N_4.

KEYWORDS: $Y_2O_3:Eu^{3+}$ Nanotube, C_3N_4, Luminescence, Composite Materials.

1. INTRODUCTION

Rare earth (RE) compounds were extensively applied to high-performance magnets, luminescence devices, catalysts, and other functional materials.[1] Most of these functions depend strongly on the composition and structure of materials. In particular, nanosized luminescent materials have attracted considerable attention since Bhargava et al. reported that doped nanocrystalline phosphors yielded high luminescence efficiencies.[2] With rapidly shrinking size, nanomaterials usually exhibit novel physical and chemical properties due to their extremely small size and relatively large specific surface areas.[3] Up to now, various techniques have been developed to synthesize desired nanostructures, such as hydrotherm, microemulsion, sol–gel, and combustion.[4] To date, there have been a number of reports in the literature about luminescence materials.[5]

It is well known that host material is an important factor to obtain high efficient luminescent properties. Among various host materials, Y_2O_3 has fine chemical and photochemical stabilities and high melting points, and can be easily doped.[6] Especially, Eu^{3+} doped Y_2O_3 phosphor is used for high efficiency cathode-ray tubes and field-emission displays because of its excellent luminescence efficiency under UV excitation.[7]

Since the discovery of carbon nanotubes by Iijima in 1991,[8] one-dimensional hollow nanostructures have sparked considerable interest in exploring new nanomaterials due to their unique architecture and unusual chemical, electrical, optical, and mechanical properties. A number of tubular materials from analogous layered structures have been reported, and related research is always one focus of nanoscience and nanotechnology.[9]

Composite materials formed by combining two or more materials could present complementary properties that have shown important technological applications.[10] It is well known that graphite-like C_3N_4 is acknowledged as one of the most stable carbon nitride allotropes materials under evironmental conditions.[11] C_3N_4 has atrracted increasing attention owing to possessing excellent mechanical, electrical, thermal, and optical properties,[12] for instance high hardness, low friction coefficient, reliable chemical inertness, and outstanding potential for energy conversion and storage. Therefore, a great deal of studies have focused on using advantages of C_3N_4 materials in various applications. Some efforts have been devoted to combining C_3N_4 with a metal or oxide to form heterojunctions because composite materials could present complementary properties.[13]

*Authors to whom correspondence should be addressed.
Emails: wanggf75@gmail.com; zhangjisen1962@163.com
Received: 27 January 2014
Accepted: 29 March 2014

Herein, we successfully prepared $Y_2O_3:Eu^{3+}/C_3N_4$ composite nanotubes by combining the hydrothermal with chemisorption method for the first time. The band gap of $Y_2O_3:Eu^{3+}/C_3N_4$ composite nanotubes become narrow with increasing the amount of C_3N_4. The charge transfer bands showed a little blue-shift after compositing with C_3N_4 in the excitation spectra of $Y_2O_3:Eu^{3+}/C_3N_4$ composite nanotubes monitored at 615 nm. More importantly, the sharp lines originating from Eu^{3+} f–f electron transitions almost vanished in the excitation spectra of $Y_2O_3:Eu^{3+}/C_3N_4$ composite nanotubes, which was attributed to the interaction between C_3N_4 and $Y_2O_3:Eu^{3+}$. The luminescence lifetimes of $Y_2O_3:Eu^{3+}$ increased by combining C_3N_4.

2. EXPERIMENTAL SECTION

2.1. Preparation of $Y_2O_3:Eu^{3+}$ Nanotubes

All of the chemicals used in this paper were analytical-grade and used as received without further purification. In a typical synthesis, 1 mL of $Ln(NO_3)_3$ aqueous solution (0.5 mol/L) was added to 4 mL deionized water, and the solution was thoroughly stirred then an aqueous solution of NaOH (0.5 M) was added into the above solution. Subsequently, the milky colloidal solution was transferred to a 50 mL Teflon-lined autoclave, and heated at 130 °C for 20 h. The systems were then allowed to cool to room temperature. The final products were collected by means of centrifugation, washed with deionized water and ethanol, dried in vacuum at 80 °C for 4 h and finally sintered at 600 °C for 2 h.

2.2. Preparation of $Y_2O_3:Eu^{3+}/C_3N_4$ Composite Nanotubes

The C_3N_4 was first prepared by heating melamine to 550 °C for 2 h in N_2 atmosphere. An appropriate amount of C_3N_4 was added into methanol then the beaker was placed in an ultrasonic bath for 30 min to completely disperse the C_3N_4. The $Y_2O_3:Eu^{3+}$ powder was added into the above solution and stirred in a fume hood for 24 h. After volatilization of the methanol, an opaque powder was obtained after drying at 100 °C in N_2 atmosphere.

2.3. Characterization

The crystal structure was analyzed by a Rigaku (Japan) D/MAX-rA X-ray diffractionmeter (XRD) equipped with graphite monochromatized Cu Kα radiation (γ = 1.541874 Å), keeping the operating voltage and current at 40 kV and 40 mA, respectively. The size and morphology of the final products were determined by using JSM-6301F scanning electron microscope and JEOL JEM-2010F transmission electron microscope operated at 200 kV. Thermogravimetry (TG) measurements were carried out on a thermal analyzer (TGA-7, Perkin-Elmer, USA) using a 2 mm internal diameter Teflon tube with a heating rate of 10 °C per minute under a flow of air. Fourier transform infrared spectra of the samples were recorded at room temperature with a Perkin-Elmer Spectrum one FTIR spectrometer using the KBr pellet method. The photoluminescence spectra were recorded with a Hitachi F-4600 fluorescence spectrophotometer at room temperature. For comparison of the luminescence properties of different samples, the luminescence spectra were measured with the same instrument parameters (2.5 nm for spectral resolution (FWHM) of the spectrophotometer and 400 V for PMT voltage). The luminescence decay curves were recorded by a Spex 1403 spectrometer under 275 nm excitation.

3. RESULTS AND DISCUSSION

3.1. Crystal Structure and Morphology

The crystal structure and particle size of products were obtained by X-ray diffraction (XRD) patterns. Figure 1(a) shows the XRD pattern of $Y_2O_3:Eu^{3+}$ nanotubes. All the diffraction peaks can be indexed to the pure cubic phase $Y_2O_3:Eu^{3+}$ (JCPDS 41-1105). No other impurity peaks were detected. Figure 1(b) shows the XRD pattern of hexagonal phase C_3N_4. The pure C_3N_4 sample had one distinct peak at 27.3°, which were indexed as (002) diffraction plane (JCPDS 87-1526). Figure 1(c) shows the XRD patterns of the $Y_2O_3:Eu^{3+}/C_3N_4$ composite nanotubes. The results indicated that $Y_2O_3:Eu^{3+}$ and C_3N_4 coexist in $Y_2O_3:Eu^{3+}/C_3N_4$ composite nanotubes. The crystal phase of $Y_2O_3:Eu^{3+}$ did not change after compositing with C_3N_4.

The size and morphology of the final products were investigated by scanning electron microscope (SEM) and transmission electron microscope (TEM). Note that we previously measured the SEM and TEM images of some $Y_2O_3:Eu^{3+}$ nanotubes prepared by the hydrothermal process, which was well in accordance with the XRD analysis results. Figures 2(a)–(c) shows the SEM images of C_3N_4 and $Y_2O_3:Eu^{3+}/C_3N_4$ (1:0.5), respectively. Obviously, C_3N_4 exhibits a sheet like morphology. The corresponding

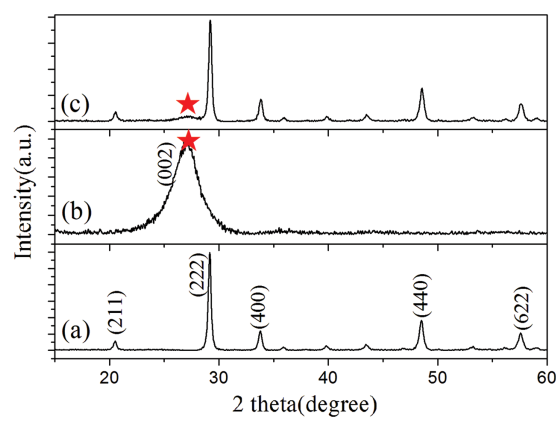

Fig. 1. XRD patterns of (a) C_3N_4, (b) $Y_2O_3:Eu^{3+}$, and $Y_2O_3:Eu^{3+}/C_3N_4$ (1:2) composite nanotubes.

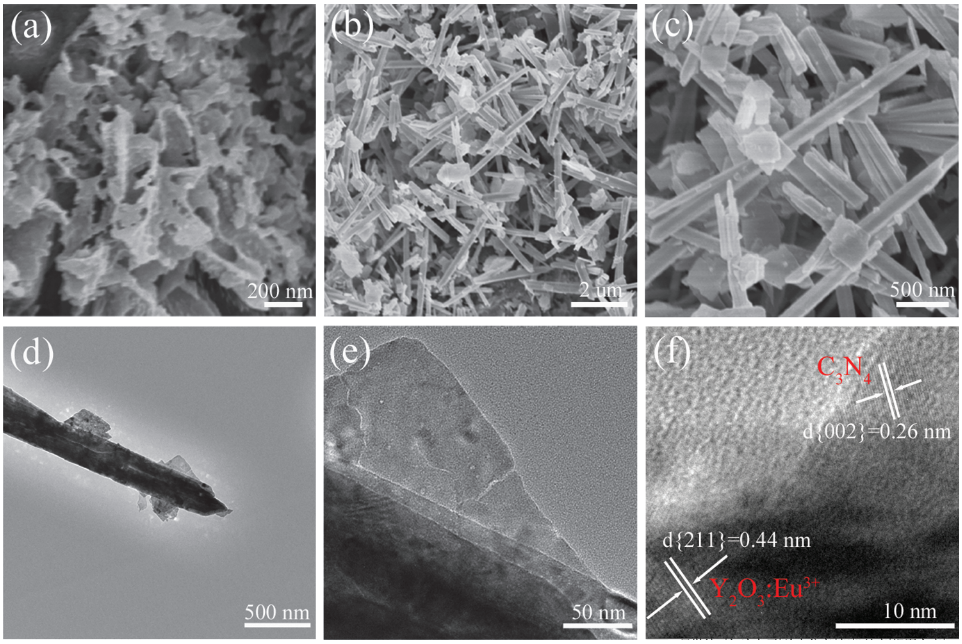

Fig. 2. SEM images of (a) C_3N_4 and (b, c) Y_2O_3:Eu^{3+}/C_3N_4 (1:0.5). (d)–(f) TEM and HRTEM images of Y_2O_3:Eu^{3+}/C_3N_4 (1:0.5).

TEM images of Y_2O_3:Eu^{3+}/C_3N_4 (1:0.5) are shown in Figures 2(d), (e). Further detailed component analysis on the Y_2O_3:Eu^{3+}/C_3N_4 composite nanotube was carried out by the high-resolution transmission electron microscope (HRTEM), as shown in Figure 2(f). Typical HRTEM image of a single composite nanotube shows two interplanar spacings of 0.44 and 0.26 nm corresponding to the ⟨211⟩ plane of cubic phase Y_2O_3:Eu^{3+} and ⟨002⟩ plane of hexagonal phase C_3N_4, respectively. The results indicated that Y_2O_3:Eu^{3+} and C_3N_4 coexist in Y_2O_3:Eu^{3+}/C_3N_4 composite nanotubes.

Figure 3 shows the IR spectra of Y_2O_3:Eu^{3+}, C_3N_4, and Y_2O_3:Eu^{3+}/C_3N_4 composite nanotubes with different Y_2O_3:Eu^{3+}/C_3N_4 mass ratios. In the spectrum of Y_2O_3:Eu^{3+}, the peak at 572 cm^{-1} can be attributed to Y–O lattice vibrations. In the spectrum of C_3N_4, the peaks at 1638 and 1238 cm^{-1} were attributed to the C═N and C–N stretching vibrations, respectively. The peak at 812 cm^{-1} was related to the s-triazine ring modes. It can be clearly seen that the main characteristic peaks of C_3N_4 and Y_2O_3 all appeared in the Y_2O_3:Eu^{3+}/C_3N_4 composite nanotubes. It is noted that the C–N (1238 cm^{-1}) stretching vibration peak moved to a higher wavenumber with increasing the amount of Y_2O_3:Eu^{3+}, suggesting the formation of Y_2O_3:Eu^{3+}/C_3N_4 composite nanotubes.

The amount of C_3N_4 could be obtained by thermogravimetric analysis (TGA), as shown in Figure 4. For pure C_3N_4, two weight loss regions could be seen in the TGA curve. The first weight loss could be attributed to the

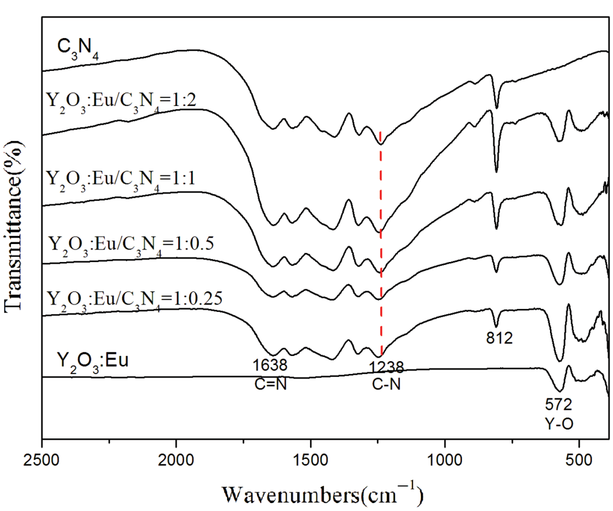

Fig. 3. Infrared spectra of Y_2O_3:Eu^{3+}, C_3N_4, and Y_2O_3:Eu^{3+}/C_3N_4 composite nanotubes with different Y_2O_3:Eu^{3+}/C_3N_4 mass ratios.

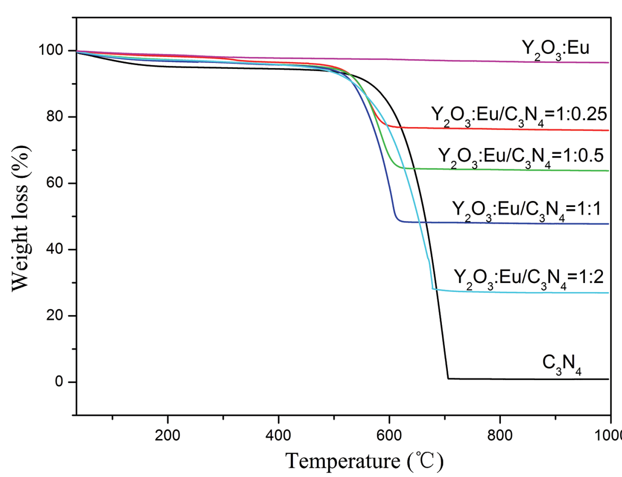

Fig. 4. TGA curves of Y_2O_3:Eu^{3+}, C_3N_4, and Y_2O_3:Eu^{3+}/C_3N_4 composite nanotubes with different Y_2O_3:Eu^{3+}/C_3N_4 mass ratios.

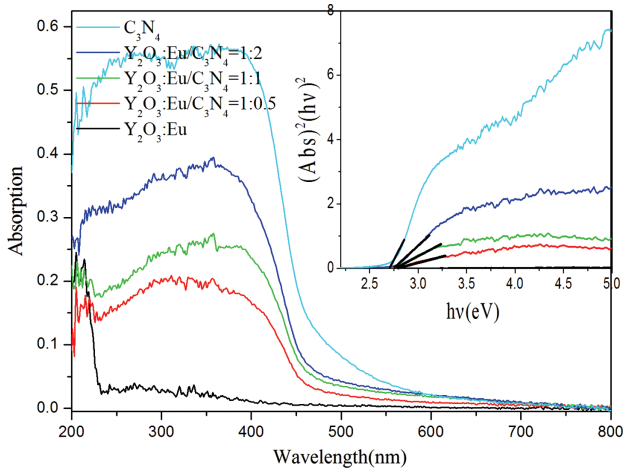

Fig. 5. UV-vis absorption spectra of $Y_2O_3:Eu^{3+}$, C_3N_4, and $Y_2O_3:Eu^{3+}/C_3N_4$ composite nanotubes with different $Y_2O_3:Eu^{3+}/C_3N_4$ mass ratios.

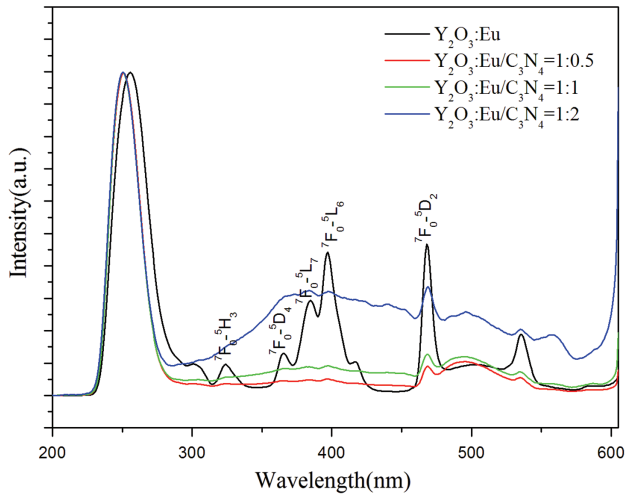

Fig. 6. The normalized excitation spectra of $Y_2O_3:Eu^{3+}$ and $Y_2O_3:Eu^{3+}/C_3N_4$ composite nanotubes with different $Y_2O_3:Eu^{3+}/C_3N_4$ mass ratios.

desorption of surface bound water. The second weight loss occurring from 500 °C to 720 °C could be assigned to the burning of C_3N_4. These two weight loss regions could be seen in all $Y_2O_3:Eu^{3+}/C_3N_4$ composite nanotubes. The amount of C_3N_4 in all $Y_2O_3:Eu^{3+}/C_3N_4$ composite nanotubes could be calculated from the second weight loss, and the results indicated that the amount of C_3N_4 was nearly consistent to the dosage of C_3N_4 added.

The optical absorption of the $Y_2O_3:Eu^{3+}$, C_3N_4, and $Y_2O_3:Eu^{3+}/C_3N_4$ composite nanotubes was conducted with a UV-vis absorption spectrometer, as shown in Figure 5. The UV-Vis absorption band increase with increasing the amount of C_3N_4. It is noted that the band edge shift was observed, and the band gap of $Y_2O_3:Eu^{3+}/C_3N_4$ composite nanotubes become narrow with increasing the amount of C_3N_4, which is benefit for the absorption of excitation light.

3.2. Luminescence Properties

Figure 6 shows the room-temperature excitation spectra of $Y_2O_3:Eu^{3+}$ and $Y_2O_3:Eu^{3+}/C_3N_4$ composite nanotubes monitored at 615 nm. The broad band extending from 200 to 300 nm is assigned to the charge transfer transitions from the 2p orbital of O^{2-} to the 4f orbital of Eu^{3+}, which is related closely to the covalency between O^{2-} and Eu^{3+} and the coordination environment around Eu^{3+}. The sharp lines in Figure 6 corresponds to the $^7F_0 \rightarrow {}^5H_3$ (~323 nm), $^7F_0 \rightarrow {}^5D_4$ (~365 nm), $^7F_0 \rightarrow {}^5G_3$ (~384 nm), $^7F_0 \rightarrow {}^5L_6$ (~397 nm), and $^7F_0 \rightarrow {}^5D_2$ (~468 nm) transitions of Eu^{3+} ions. Obviously, the charge transfer bands showed a little blue-shift after compositing with C_3N_4. More interesting, the sharp lines originate from Eu^{3+} f–f electron transitions almost vanished in the excitation spectra of $Y_2O_3:Eu^{3+}/C_3N_4$ composite nanotubes. We suggest that the change of excitation spectra between $Y_2O_3:Eu^{3+}$ and $Y_2O_3:Eu^{3+}/C_3N_4$ was attributed to the interaction between C_3N_4 and $Y_2O_3:Eu^{3+}$. Figure 7 shows the emission spectra of $Y_2O_3:Eu^{3+}$ and $Y_2O_3:Eu^{3+}/C_3N_4$ composite nanotubes with different $Y_2O_3:Eu^{3+}/C_3N_4$ mass ratios. The luminescence was dominated by $^5D_0 \rightarrow {}^7F_2$ transition.

Figure 8 shows the excitation spectra of $Y_2O_3:Eu^{3+}/C_3N_4$ (1:0.5) composite nanotubes monitored at different emission wavelengths. Only one excitation band centered at ~250 nm was observed in the excitation spectrum of $Y_2O_3:Eu^{3+}/C_3N_4$ (1:0.5) composite nanotubes monitored at 596 and 633 nm, which was different from that monitored at 615 nm. This is a normal phenomenon when the material has multiple luminescence centers or emitting states. Figure 9 shows the emission spectra of $Y_2O_3:Eu^{3+}/C_3N_4$ (1:0.5) composite nanotubes excited at 250, 465, and 494 nm. It can be observed that the emission

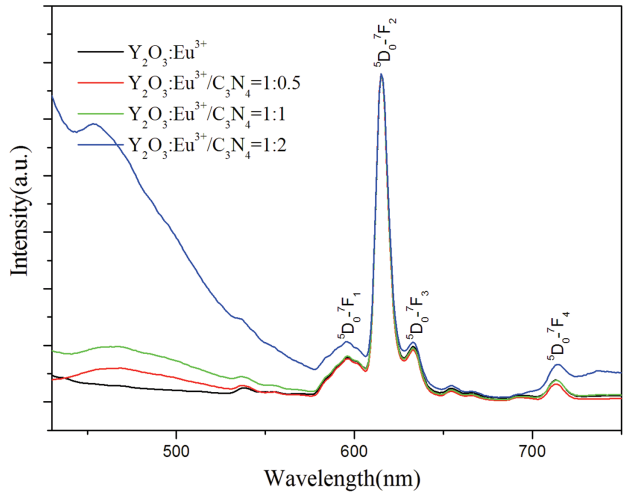

Fig. 7. The normalized emission spectra of $Y_2O_3:Eu^{3+}$ and $Y_2O_3:Eu^{3+}/C_3N_4$ composite nanotubes with different $Y_2O_3:Eu^{3+}/C_3N_4$ mass ratios.

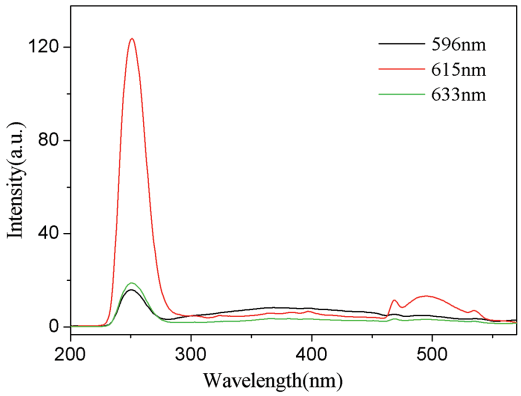

Fig. 8. Excitation spectra of $Y_2O_3:Eu^{3+}/C_3N_4$ (1:0.5) composite nanotubes monitored at different emission wavelengths.

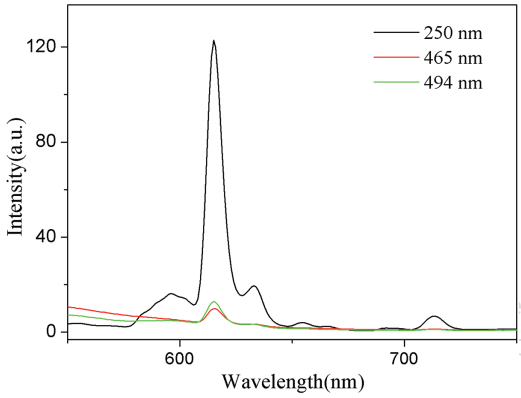

Fig. 9. Emission spectra of $Y_2O_3:Eu^{3+}/C_3N_4$ (1:0.5) composite nanotubes excited at different wavelengths.

intensities were the strongest when the excitation was performed at 250 nm.

In order to explain the interaction between $Y_2O_3:Eu^{3+}$ and C_3N_4, the luminescence decay curves of the $^5D_0 \rightarrow {}^7F_2$ transition for the $Y_2O_3:Eu^{3+}$ and $Y_2O_3:Eu^{3+}/C_3N_4$ composite nanotubes were recorded, as shown in Figure 10. It is noted that the decay curve cannot be fitted with the single exponential function, while a biexponential function may reproduce the decay data well and lead to two

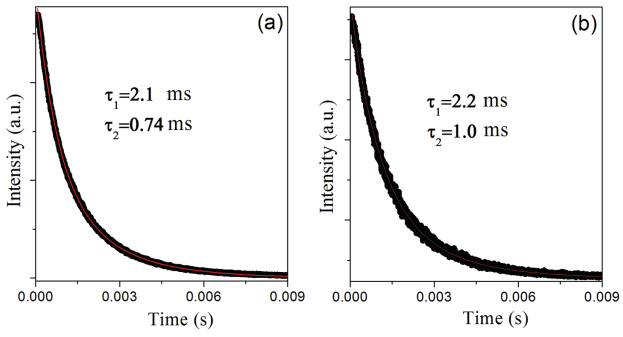

Fig. 10. The luminescence decay curves for the $Y_2O_3:Eu^{3+}$ and $Y_2O_3:Eu^{3+}/C_3N_4$ (1:0.5) composite nanotubes.

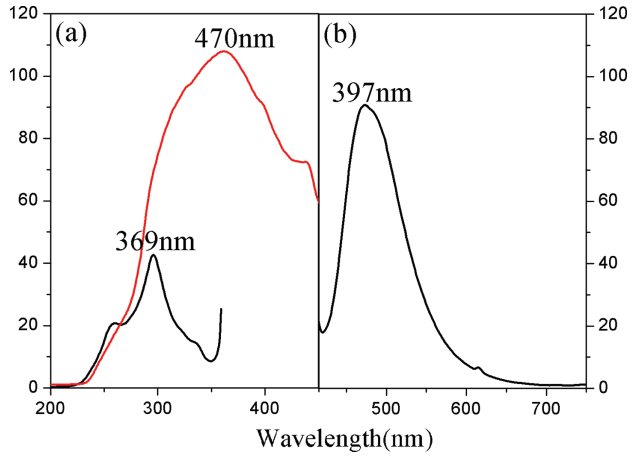

Fig. 11. (a) Excitation and (b) emission spectra of $Y_2O_3:Eu^{3+}/C_3N_4$ (1:0.5) composite nanotubes.

lifetimes of 2.1 and 0.74 ms for $Y_2O_3:Eu^{3+}$ nanotubes, and 2.2 and 1.0 ms for $Y_2O_3:Eu^{3+}/C_3N_4$ (1:0.5) composite nanotubes. It is well known that the lifetime t is determined by the radiative transition rate and the nonradiative transition rate. The nonradiative relaxation rate is related to surface defects. We suggested that the longer lifetimes (t_1) correspond to the $^5D_0$ level of the Eu^{3+} ions inside the nanotubes. t_2 should correspond to the $^5D_0$ level of the Eu^{3+} ions near the surface. Here, luminescence lifetimes of $Y_2O_3:Eu^{3+}$ increased by combining C_3N_4.

Figure 11(a) shows the excitation spectra of $Y_2O_3:Eu^{3+}/C_3N_4$ (1:0.5) composite nanotubes monitored at 369 and 467 nm. Figure 11(b) shows the emission spectrum of $Y_2O_3:Eu^{3+}/C_3N_4$ (1:0.5) composite nanotubes excited at 397 nm. Obviously, a very strong emissions band centered at 470 nm was observed, which corresponds to the transition from C_3N_4.[14]

4. CONCLUSIONS

In conclusion, $Y_2O_3:Eu^{3+}/C_3N_4$ composite nanotubes were successfully synthesized for the first time. The infrared spectra indicated that the C–N (1238 cm^{-1}) stretching vibration peak moved to a higher wavenumber with increasing the amount of $Y_2O_3:Eu^{3+}$, suggesting the formation of $Y_2O_3:Eu^{3+}/C_3N_4$ composite nanotubes. The band gap of $Y_2O_3:Eu^{3+}/C_3N_4$ composite nanotubes become narrow with increasing the amount of C_3N_4. In the excitation spectra of $Y_2O_3:Eu^{3+}/C_3N_4$ composite nanotubes monitored at 615 nm, the charge transfer bands showed a little blue-shift after compositing with C_3N_4. More importantly, the sharp lines originate from Eu^{3+} f–f electron transitions almost vanished in the excitation spectra of $Y_2O_3:Eu^{3+}/C_3N_4$ composite nanotubes. We suggest that the change of excitation spectra between $Y_2O_3:Eu^{3+}$ and $Y_2O_3:Eu^{3+}/C_3N_4$ was attributed to the interaction between C_3N_4 and $Y_2O_3:Eu^{3+}$. The excitation spectrum of $Y_2O_3:Eu^{3+}/C_3N_4$ (1:0.5) composite nanotubes monitored

at 615 nm was different from those monitored at 596 and 633 nm, indicating that the material has multiple luminescence centers or emitting states. The decay curve of Y_2O_3:Eu^{3+} and Y_2O_3:Eu^{3+}/C_3N_4 composite nanotubes cannot be fitted with the single exponential function, while a biexponential function may reproduce the decay data well. The luminescence lifetimes of Y_2O_3:Eu^{3+} increased by combining C_3N_4.

Acknowledgments: This work was supported by the National Natural Science Foundation of China (11174276 and 21171052), the Program for New Century Excellent Talents in University of Ministry of Education of China (NCET-11-0959), the Postdoctoral Science Foundation of Heilongjiang Province (LBH-Q11009), Program for Innovative Research Team in University (IRT-1237), Heilongjiang Province Natural Science Foundation of Key Projects (ZD201301), Harbin Technological Innovation Talent of Special Funds (RC2013QN017028), and Innovative Project of Postgraduate of Heilongjiang Province.

References and Notes

1. (a) G. Wang, Q. Peng, and Y. Li, *Acc. Chem. Res.* 44, 322 (**2011**); (b) S. Eliseeva and J. Bünzli, *Chem. Soc. Rev.* 39, 189 (**2010**); (c) J. Bünzli and C. Piguet, *Chem. Soc. Rev.* 34, 1048 (**2005**); (d) Y. Li, G. Wang, K. Pan, Y. Qu, S. Liu, and L. Feng, *Dalton Trans.* 42, 3366 (**2013**); (e) L. Wang and Y. Li, *Nano Lett.* 6, 1645 (**2006**).
2. (a) Y. Li, G. Wang, K. Pan, B. Jiang, C. Tian, W. Zhou, and H. Fu, *J. Mater. Chem.* 22, 20381 (**2012**); (b) F. Wang and X. G. Liu, *Chem. Soc. Rev.* 38, 976 (**2009**); (c) G. Wang, W. Qin, J. Zhang, J. Zhang, Y. Wang, C. Cao, L. Wang, G. Wei, P. Zhu, and R. Kim, *J. Phys. Chem. C* 112, 12161 (**2008**); (d) X. Bai, H. Song, G. Pan, Y. Lei, T. Wang, X. Ren, S. Lu, B. Dong, Q. Dai, and L. Fan, *J. Phys. Chem. C* 111, 13611 (**2007**); (e) G. Wang, Q. Peng, and Y. Li, *Chem. Commun.* 46, 7528 (**2010**).
3. (a) L. Li, R. Zhuang, L. Yin, K. Zheng, W. Qin, P. Selvin, and Y. Lu, *Augew. Chem. Int. Ed.* 51, 6121 (**2012**); (b) M. Cao, Y. Wang, Y. Qi, C. Guo, and C. Hu, *J. Solid State Chem.* 177, 2205 (**2004**); (c) A. Patra, C. S. Friend, R. Kapoor, and N. Prasad, *J. Phys. Chem. B* 106, 1909 (**2002**).
4. (a) X. Wang and Y. Li, *Chem. Eur. J.* 9, 5627 (**2003**); (b) L. Wang and Y. Li, *Chem. Mater.* 19, 727 (**2007**); (c) M. Schwuger, K. Stickdom, and R. Schomacker, *Chem. Rev.* 95, 849 (**1995**); (d) R. Yan and Y. Li, *Adv. Funct. Mater.* 15, 763 (**2005**).
5. (a) C. Zhang and J. Lin, *Chem. Soc. Rev.* 41, 7938 (**2012**); (b) H. Mai, Y. Zhang, L. Sun, and C. Yan, *J. Phys. Chem. C* 111, 13721 (**2007**); (c) S. Li, X. Zhang, Z. Hou, Z. Cheng, P. Ma, and J. Lin, *Nanoscale* 4, 5619 (**2012**).
6. J. Zhang, S. Wang, L. An, M. Liu, and L. Chen, *J. Lumin.* 122, 8 (**2007**).
7. (a) Z. Xia and R. Liu, *J. Mater. Chem.* 22, 15183 (**2012**); (b) Z. Xu, Y. Gao, T. Liu, L. Wang, S. Bian, and J. Lin, *J. Mater. Chem.* 22, 21695 (**2012**); (c) Z. Xia, J. Zhuang, and L. Liao, *Inorg. Chem.* 51, 7202 (**2012**).
8. S. Iijima, *Nature* 354, 56 (**1991**).
9. C. Wu, W. Qin, G. Qin, D. Zhao, J. Zhang, S. Huang, S. Lü, H. Liu, and H. Lin, *Appl. Phys. Lett.* 82, 520 (**2003**).
10. (a) R. Das, S. Bhat, S. Banerjee, C. Aymonier, A. Loppinet-Serani, P. Terech, U. Maitra, G. Raffy, J. Desvergne, and A. Guerzo, *J. Mater. Chem.* 21, 2740 (**2011**); (b) B. Jiang, G. Tian, W. Zhou, J. Wang, Y. Xie, Q. Pan, Z. Ren, Y. Dong, D. Fu, J. Han, and H. Fu, *Chem. Eur. J.* 17, 8379 (**2011**).
11. R. Comparelli, E. Fanizza, M. L. Curri, P. D. Cozzoli, G. Mascolo, and A. Agostiano, *Appl. Catal. B* 60, 1 (**2005**).
12. G. Yu, J. Gao, J. C. Hummelen, F. Wudl, and A. J. Heeger, *Science* 270, 1789 (**1995**).
13. G. Wang, Y. Li, B. Jiang, K. Pan, N. Fan, Q. Feng, Y. Chen, and C. Tian, *Chem. Comm.* 47, 8019 (**2011**).
14. Y. Zhang, Q. Pan, G. Chai, M. Liang, G. Dong, Q. Zhang, and J. Qiu, *Scientific Reports* 3, 1943 (**2013**).

ARTICLE